Wang-Landau sampling with logarithmic windows for continuous models

Y. L. Xie, P. Chu, Y. L. Wang, J. P. Chen, Z. B. Yan, and J.-M. Liu*
Laboratory of Solid State Microstructures, Nanjing University, Nanjing 210093, China
(Received 26 September 2013; published 29 January 2014)

We present a modified Wang-Landau sampling (MWLS) for continuous statistical models by partitioning the energy space into a set of windows with logarithmically shrinking width. To demonstrate its necessity and advantages, we apply this sampling to several continuous models, including the two-dimensional square *XY* spin model, triangular J_1-J_2 spin model, and Lennard-Jones cluster model. Given a finite number of bins for partitioning the energy space, the conventional Wang-Landau sampling may not generate sufficiently accurate density of states (DOS) around the energy boundaries. However, it is demonstrated that much more accurate DOS can be obtained by this MWLS, and thus a precise evaluation of the thermodynamic behaviors of the continuous models at extreme low temperature ($k_BT < 0.1$) becomes accessible. The present algorithm also allows efficient computation besides the highly reliable data sampling.

DOI: 10.1103/PhysRevE.89.013311 PACS number(s): 05.10.Ln, 64.60.Cn

I. INTRODUCTION

As an important and efficient algorithm for Monte Carlo (MC) simulation, the Wang-Landau sampling (WLS) [1–3] has been extensively applied to various models in statistical physics and biophysics recently [4,5]. For conventional metropolis MC (MMC) approaches, the random walk is prone to fall into traps at local energy minima in models with complex energy landscape. The WLS can ingeniously escape from such difficulties, for it tracks the sampling of the density of states (DOS) directly. Once we obtain the DOS spectrum over the whole energy space for a statistical system, thermodynamic observables including the internal energy and heat capacity can be calculated logically, with no need to track the parameter (e.g., temperature T) -dependent sampling sequence which can be tedious and relatively inefficient.

As a kind of importance sampling, the WLS chooses the transition probability p of a random walk in the energy space from a state (configuration) with energy level E_1 to that with energy level E_2 as $p(E_1 \to E_2) = \min[1, g(E_1)/g(E_2)]$, where $g(E_1)$ and $g(E_2)$ are the instant DOS at E_1 and E_2, respectively. This WLS procedure starts from a random configuration with initial DOS $g(E) = 1$ and histogram $H(E) = 0$ for all energy levels, where histogram $H(E)$ is used as a collector of the number of visits at energy level E. For a trial walk from a state at level E_1 to another one at E_2, the event is accepted at probability $p(E_1 \to E_2)$. Then the configuration is updated and the DOS $g(E_2) \to g(E_2)f$ and histogram $H(E_2) \to H(E_2) + 1$ are imposed. Otherwise, $g(E_1) \to g(E_1)f$ and $H(E_1) \to H(E_1) + 1$ are updated. Here, parameter f is the modification factor and usually $f > 1.0$. After sufficient trial events, the initially scattered histogram spectrum $H(E)$ gradually becomes sufficiently "flat", completing one iteration cycle of the simulation. Then one resets this spectrum to 0 and updates f as $f \to f^{1/2}$ for the next iteration cycle. The WLS procedure goes on until $f < f_{\text{lim}}$, where f_{lim} is the limit of modification factor very close to 1.0; for example, $f_{\text{lim}} = 1 + 10^{-7}$ is often taken.

Nevertheless, it is well known that for a statistical system with either the DOS minimal or the maximal DOS negative derivative over energy (the maximal DOS decreasing rate) on the bottom and top boundaries of energy space, which is usually the case for most statistical models, such a procedure of importance sampling will give rise to relatively big errors for the DOS on these boundary states (the bottom boundary state is the ground state). One may call this phenomenon *the boundary effect*. To understand this issue, we use E_{min} and E_{mid} to denote the energy levels on the ground state and on the middle range of the energy space, respectively. One example is shown in Fig. 1(a) where the DOS spectrum $g(E)$ for a simple spin model is plotted. In this case, one has a very large $g(E_{\text{mid}})/g(E_{\text{min}})$ ratio, and most of the trial walks from E_{min} to E_{mid} are rejected, yet the acceptance rate for the boundary states near the ground state is so low that these states are hard to access. This implies a big sampling error even though the modification factor f is very close to 1. Surely, this sampling error can be reduced if a huge number of trial events are taken with very low sampling efficiency.

At the same time, such a large $g(E_m)/g(E_{\text{min}})$ ratio makes it extremely difficult for a random walk to find a path bridging the states E_{mid} and state E_{min} in the energy space. The whole sampling sequence has to use plenty of CPU time in order to obtain a "flat" histogram $H(E)$ which can even be an impossible mission in practical simulations. This issue raises some difficulties when we employ the WLS to obtain the $g(E)$ spectrum with high precision at the boundary states. For example, it is known that the ratio $g(E_{\text{mid}})/g(E_{\text{min}})$ increases with the lattice size N. We take the Ising spin model on a square lattice with dimensions of 100×100 as an example, where $g(E_1)/g(E_0) \sim N = 10^4$, and E_0 and E_1 are the energy levels of the ground state and the first low-energy excited state. Such a big gap somehow makes the ground state rarely reachable if not unreachable, and the lattice may be trapped in this first low-energy excited state for a big number of CPU trials. For avoiding this difficulty, usually one chooses an energy cutoff E_c which is slightly higher than E_{min}, so that the low-energy states instead of the lowest-energy state (ground state) can be reasonably accessed in finite and affordable CPU time. These low-energy states are treated as approximations to the ground state.

*Corresponding author: liujm@nju.edu.cn

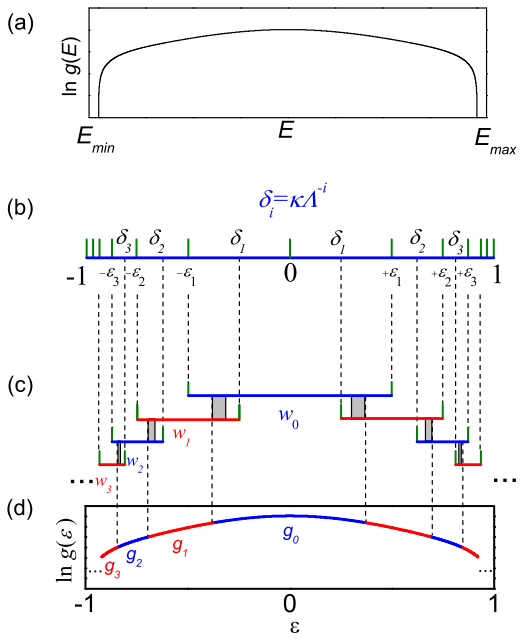

FIG. 1. (Color online) (a) A sketch of the DOS spectrum $g(E)$ for a typical continuous spin model. (b) A logarithmic partition of the normalized energy space with discretization parameters Λ ($\Lambda > 1$) and κ. (c) A schematic drawing of the window set w_i with lines to guide the eyes. (d) Joint DOS $g(\varepsilon)$ from the modified algorithm. See text.

Recently, quite a few elaborate algorithms have been proposed to accelerate the WLS and to enhance the data precision, including the WLS with self-adaptive range [6], the WLS with adaptive windows [7], the parallel WLS based on the replica-exchange framework [8], and so on [9,10]. A number of issues including the aforementioned problems are substantially avoided. However, the relatively big errors at the boundary states for continuous models with extremely low-T phase transitions remain to be an issue. It is known that continuous models like the Heisenberg spin model and in-plane two-dimensional (2D) XY spin model have continuous energy distribution. These models do exhibit phase transitions at extremely low T [9,11–13], which, however, are hard if not impossible to access using the conventional WLS, while an accurate evaluation of the $g(E)$ spectrum is extremely critical.

For the simplest situation, we consider the 2D XY spin model only with the nearest neighbor interactions. Fortunately, an analytical solution for the boundary DOS is available, given some reasonable approximations [11]. This solution presents a sound platform on which any algorithm dealing with this issue can be checked with high precision. Given a sufficiently accurate set of DOS data not only near the boundaries, a series of thermodynamic observables evaluated from the DOS spectrum over the whole energy space can be calculated. It should be mentioned that even for those simple continuous models with extremely low phase transitions such as the J_1-J_2 spin model on triangular lattice [12], the analytical expression is available only in the very narrow range from the boundary states. It will be found that the as-obtained $g(E)$ from the conventional WLS loses its consistency with the analytical solution (expression) in this range. This is the motivation for proposing an alternative approach to figure out this problem here.

In this article, we will first address the issue of remarkable errors at the boundaries of the energy space. Then we introduce a modified Wang-Landau sampling (MWLS) scheme based on the conventional WLS (CWLS), aiming at the DOS spectrum of continuous models with sufficiently high accuracy. This allows an accurate calculation of the thermodynamic observables at extremely low temperature. It will be demonstrated that this MWLS is indeed powerful in enhancing the data precision and computation efficiency for continuous statistical models.

II. LOGARITHMIC WINDOW STRATEGY

A. Definition

In this section, we propose this MWLS scheme. First, we make a brief discussion on the $g(E)$ over the whole energy space. For continuous models, the energy distribution between $E_{\min}$ and $E_{\max}$ is continuous and $g(E)$ is also continuous, as schematically shown in Fig. 1(a), where $E_{\max}$ is the top boundary energy. As a general characteristic, function $\ln[g(E)]$ always drops down rapidly as E is close to $E_{\min}$ and $E_{\max}$, respectively [11,14]. For a better description of the $g(E)$, in practical simulation we discretize the energy space into a series of windows. A reasonable scheme is to discretize it by a set of width-varying windows: *broad windows on the energy range where the $g(E)$ varies slowly and narrow windows on the energy range where the $g(E)$ varies rapidly*. This scheme seems to be similar to the renormalization approach but here it is much simpler. We may name it as the logarithmic discretization scheme of the energy space.

B. Dimensionless normalization of energy space

We start from the WLS with windows, which are usually employed for large-size systems and have separate sampling procedures [2,7]. First, we rescale the energy space via the following dimensionless transform:

$$\varepsilon = (E-\alpha)/\beta \Leftarrow \begin{cases} \alpha = (E_{\max}+E_{\min})/2 \\ \beta = (E_{\max}-E_{\min})/2 \end{cases}, \qquad (1)$$

where $E_{\min}$ and $E_{\max}$ are again the bottom and top boundaries of the energy space, respectively. By this transform, the energy space is transferred into dimensionless form $\varepsilon \in [-1,1]$, as shown in Fig. 1(b).

Subsequently, we partition the energy space into two sets of "windows" (the set with $\varepsilon > 0$ and the set with $\varepsilon < 0$) with logarithmically shrinking width. The widths and border coordinates of the two sets of windows, as labeled in Fig. 1(b), can be expressed as

$$\delta_i = \kappa\Lambda^{-i}, \quad \pm\varepsilon_i = \pm\sum_{j=1}^{i}\kappa\Lambda^{-j}$$
$$= \pm(1-\Lambda^{-i}) \ (i = 1,2,3\cdots), \qquad (2)$$

where Λ is the discretization parameter and $\kappa = \Lambda - 1$. Λ should be a number larger than 1. In our simulation, $\Lambda = 2$ is chosen for simplicity and then $\kappa = 1$.

Based on the above window discretization scheme, we employ the CWLS procedure for each window. Here, each window is discretized into an equal number of bins (bin number n_w). The CWLS generate the $g(\varepsilon)$ spectrum for each of these windows. Subsequently, we combine these $g(\varepsilon)$ spectra together to constitute the spectrum $g(\varepsilon)$ over the whole space $\varepsilon \in [-1,1]$. Unfortunately, the above scheme does not work well, since different windows have different interval (bin) widths, leading to non-negligible energy scale dispersion. In addition, similar to a previously mentioned reason, each of these windows has its own *boundary effect*, i.e., relatively big errors at the two borders of the window [13,15]. The consequence is that the obtained $g(\varepsilon)$ data at the border between two neighboring windows do not match very well. Ideally, a simple combination of the $g(\varepsilon)$ series can be performed by satisfying the following conditions in sequence:

$$\begin{cases} g(\varepsilon \to \varepsilon_i + 0) = g(\varepsilon \to \varepsilon_i - 0) \\ g(\varepsilon \to -\varepsilon_i + 0) = g(\varepsilon \to -\varepsilon_i - 0) \end{cases}, (i = 1,2,3\cdots), \quad (3)$$

The as-obtained $g(\varepsilon)$ spectrum is not a smooth curve but with a number of features which are physically unreasonable. In other words, spectrum $g(\varepsilon)$ shows relatively big errors at the borders of each window.

C. Renormalization of energy space

In order to exclude these unphysical features and obtain a high-precision $g(\varepsilon)$ spectrum, one may reorganize the logarithmic windows in the practical simulation so that these windows are partially overlapped at their borders, as shown in Fig. 1(c). Such reorganization may have more than one scheme. We propose a simple scheme, as shown in Figs. 1(c) and 1(d), and more clearly shown in Fig. 2. We assign window w_0 with its midpoint located at $\varepsilon = 0$ and its width as $w_0 = 2\delta_1 = 2\kappa\Lambda^{-1}$. The partition rule for the subsequent windows can be described by the midpoint coordinate and width of the ith window w_i at the two sides of $\varepsilon = 0$:

$$\pm\varepsilon_i = \pm(1 - \Lambda^{-i}), \quad w_i = \kappa\Lambda^{-i} \quad (i = 1,2,3\cdots). \quad (4)$$

It is seen that any pair of neighboring windows are partially overlapped. Such an overlap allows the above addressed DOS data mismatch at their border and the other border effects to be excluded when the DOS data of the two windows are combined. Without losing the generality, we take two neighboring windows w_i and w_{i+1} in the $\varepsilon < 0$ side for an illustration, while the $\varepsilon > 0$ side is no longer discussed subsequently. It is noted that the overlapping width of windows w_i and w_{i+1} is $\kappa\Lambda^{-(i+2)}$. The DOS data of the two windows are denoted as $g_i(\varepsilon)$ and $g_{i+1}(\varepsilon)$, respectively. They are defined

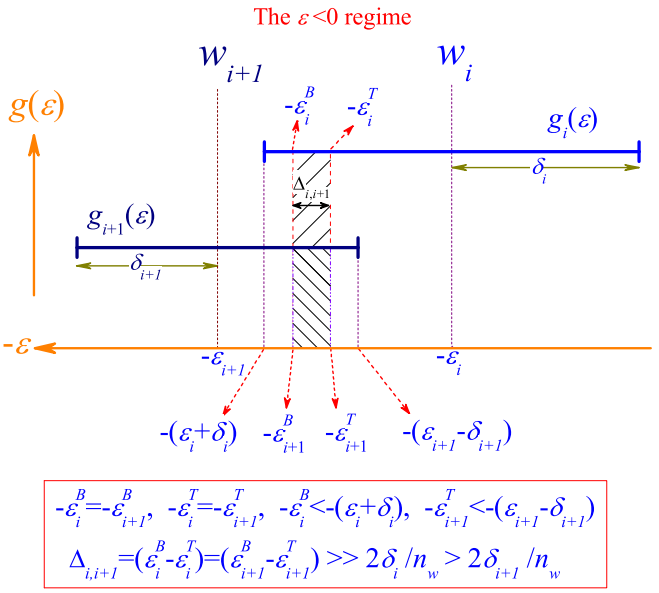

FIG. 2. (Color online) A close view of two neighboring windows and definition of a series of parameters for the modified algorithm. See text.

in corresponding finite ε subspaces:

$$g(\varepsilon) = \begin{cases} g_i(\varepsilon), & -(\varepsilon_i + \frac{1}{2}w_i) < \varepsilon < -(\varepsilon_i - \frac{1}{2}w_i) \\ g_{i+1}(\varepsilon), & -(\varepsilon_{i+1} + \frac{1}{2}w_{i+1}) < \varepsilon < -(\varepsilon_{i+1} - \frac{1}{2}w_{i+1}) \end{cases}, \quad (5)$$

Clearly, $g_i(\varepsilon)$ and $g_{i+1}(\varepsilon)$ do not match over the overlapping range and usually $g_i(\varepsilon) > g_{i+1}(\varepsilon)$. In this case, Eq. (3) cannot be simply used due to the *boundary effect*. To make $g_i(\varepsilon)$ and $g_{i+1}(\varepsilon)$ match with each other, we perform the following simple and straightforward modification. Figure 2 shows two neighboring windows w_i and w_{i+1}. The left (bottom) border of window w_i is located at $-\varepsilon = -(\varepsilon_i + \delta_i)$ while the right (top) border of window w_{i+1} is at $-\varepsilon = -(\varepsilon_{i+1} - \delta_{i+1})$. Clearly, one has $(\varepsilon_i + \delta_i) > (\varepsilon_{i+1} - \delta_{i+1})$, and can thus choose the shade ranges from the two windows respectively, satisfying

$$\begin{cases} -\varepsilon_i^B < -(\varepsilon_i + \delta_i) \\ -\varepsilon_{i+1}^T < -(\varepsilon_{i+1} - \delta_{i+1}) \end{cases}, \begin{cases} -\varepsilon_i^B = -\varepsilon_{i+1}^B \\ -\varepsilon_i^T = -\varepsilon_{i+1}^T \end{cases}, \quad (6)$$

$$\Delta_{i,i+1} = \left(\varepsilon_i^B - \varepsilon_i^T\right) = \left(\varepsilon_{i+1}^B - \varepsilon_{i+1}^T\right) \gg \frac{2\delta_i}{n_w} > \frac{2\delta_{i+1}}{n_w},$$

where superscripts B and T label the bottom and top borders of the corresponding window, respectively. In a typical case, we take $\Delta_{i,i+1} = 20\delta_i/n_w$. By this choice, we can define the momentum S_i and S_{i+1}:

$$\begin{cases} S_i = \int g_i(\varepsilon)d\varepsilon, -\varepsilon_i^B < -\varepsilon < -\varepsilon_i^T \\ S_{i+1} = \int g_{i+1}(\varepsilon)d\varepsilon, -\varepsilon_{i+1}^B < -\varepsilon < -\varepsilon_{i+1}^T \end{cases}, i = 0,1,2,\cdots. \quad (7)$$

By setting $S_{i+1} = A_{i,i+1}S_i$, one has the iteration transform

$$g_{i+1}(\varepsilon) = A_{i,i+1}g_i(\varepsilon), i = 1,2,3,\cdots. \quad (8)$$

The above iteration process eventually generates a full-scale $g(\varepsilon)$ spectrum over the whole $\varepsilon < 0$ space. The same procedure can be applied to the $\varepsilon > 0$ space, although the $g(\varepsilon)$ spectrum

over the $\varepsilon > 0$ space does not make a substantial contribution to the low-energy excited states at extremely low-T range. Here it should be noted that the $g_i(\varepsilon)$ data over $-\varepsilon < -\varepsilon_i^B$ and the $g_{i+1}(\varepsilon)$ data over $-\varepsilon > -\varepsilon_{i+1}^B$ can be safely removed. The as-obtained $g(\varepsilon)$ spectrum by this renormalization procedure is schematically shown in Fig. 1(d).

It should be mentioned that this scheme is flexible and the principle is to exclude the big errors in $g(\varepsilon)$ at the two ends of each window by a smoothing procedure. This flexibility does not influence the precision of the calculated data.

D. Procedure of simulation

Based on the above scheme, we can obtain the smooth $g(\varepsilon)$ spectrum. Here we only describe the computation procedure for the $\varepsilon < 0$ side. Initially, we need a "key", i.e., a configuration in a specific window to start up the WLS. Usually, a random configuration is a preferable one. We start from the window w_0 [Fig. 1(c)] and proceed from a random configuration with energy ε satisfying $-\Lambda^{-1} \leqslant \varepsilon \leqslant \Lambda^{-1}$. The WLS random walk is restricted only in this window. For generalization consideration, we set that energy ε_{try} of the trial configuration must fall into the energy interval $[\varepsilon_{lw}, \varepsilon_{uw}]$, with ε_{lw} and ε_{uw} the lower and upper energy borders of the assigned window, respectively. If this condition is not satisfied, discard the trial configuration and update g(ε) and $H(\varepsilon)$ at this energy level, according to Ref. [15], and then have another try. In consequence, we perform the CWLS procedure to obtain the $g(\varepsilon)$ spectrum in $[\varepsilon_{lw}, \varepsilon_{uw}]$. When ε_{try} moves in the interval $[\varepsilon_{lw}, \varepsilon_{lw} + \delta\varepsilon]$, the trial spin configuration is saved as the key to start up the WLS procedure in the next window; here $\delta\varepsilon$ is small with respect to the window width, typically $\delta\varepsilon = (\varepsilon_{uw} - \varepsilon_{lw})/8$.

We set the same control parameters for the simulations using both CWLS and MWLS. We say that the $H(\varepsilon)$ spectrum is "flat" when the divergence from its average over the whole energy space is less than 10%. The limit of modification factor $f_{\text{lim}} = 1 + 10^{-7}$. For the CWLS, the bin number is usually 4000 unless stated otherwise and the low-energy cutoff is $\varepsilon_c > -1.0$. For the MWLS, if $f < f_{\text{lim}}$, simulation in the present window ends and a new WLS procedure in the next window begins. The number of logarithmic windows is $N_w \geqslant 12$ while the bin number in each window is $n_w = 600$, and then the total bin number is $n_w N_w$. In this case, the low-energy cutoff ε_c is defined by relation $\ln(\varepsilon_c + 1) = -N_w \ln\Lambda = -N_w \ln 2$, implying that $\varepsilon_c \to -1.0$ with increasing N_w.

III. MODELS AND SIMULATION RESULTS

In order to demonstrate the advantages of this MWLS algorithm, we apply it to three well known continuous models, i.e., the square XY spin model, the J_1-J_2 spin model on triangular lattice, and the Lennard-Jones cluster.

A. Square XY spin model

We first consider the plane square XY spin model. The Hamiltonian is $H = J \sum_{<i,\,j>} \cos(\theta_{ij})$, where the summation goes over the nearest neighbors on a square lattice with periodic boundary conditions and θ_{ij} is the angle difference between the spins on site i and its neighbor site j, $\theta_{ij} = \theta_i - \theta_j$. In our simulation the exchange interaction J is set as -1.0 for simplicity. We have $E_{\min} = -2N$ where $N = LL$ (L is the width of the lattice) is the spin number and also the lattice size, and $E_{\max} = 2N$. Then the whole energy space is rescaled via Eq. (1) with $\alpha = 0$, $\beta = 2N$.

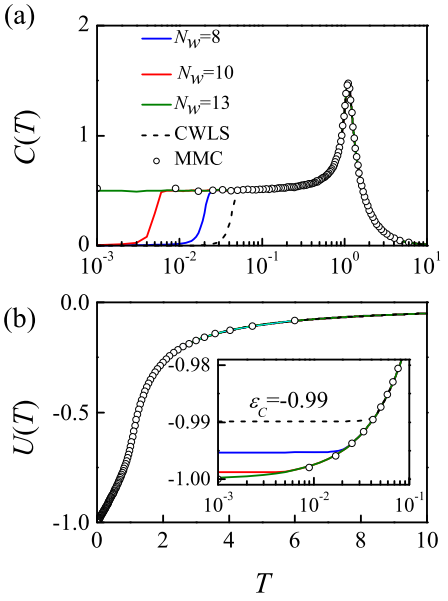

FIG. 3. (Color online) Calculated heat capacity $C(T)$ (a) and internal energy $U(T)$ (b) from the simulated DOS for the two-dimensional square XY model with $N = 16 \times 16$ square, using the three different algorithms (MMC, CWLS, and MWLS with $N_w = 8$, 10, and 13), respectively.

It is noted again that we only calculate the $g(\varepsilon)$ spectrum at $\varepsilon < 0$, because we focus our attention on the low-T thermodynamics, and the influence of $g(\varepsilon > 0)$ on the low-T phase transitions is negligible. For the MWLS, given a relatively big N_w ($N_w \geqslant 12$), it is seen that the cutoff is very close to the ground state $\varepsilon = -1.0$ and thus highly reliable. The simulated results at three different N_w values (8, 10, 13) are shown in Fig. 3, in which the data from the CWLS and MMC methods are shown too for comparison. The $\varepsilon_c = -0.99$ is taken for the CWLS due to the limited computation capacity. The MMC is performed upon a sequence of 100 temperature points from $T = 6.0$ to $T = 0.001$, using 10^6 MC steps to relax and taking 10^5 samples from the next 3×10^6 MC steps at each T point.

It is seen that the three algorithms produce the overlapped $C(T)$ peaks, while the difference appears below this critical point, as shown in Fig. 3(a). The rigorous prediction [11] is $C(T) \to 0.5$ at $T \to 0$, as confirmed here by the MMC data. Unfortunately, the $C(T)$ data from the CWLS exhibit the dropdown point at $T \sim 0.05$. Instead, the MWLS produces much better data and the dropdown point shifts rapidly towards the $T \to 0$ with increasing N_w. The $C(T)$ data at $N_w = 13$ perfectly agree with the MMC data and also with the rigorous prediction (to be shown below).

The evaluated internal energy $U(T)$ data from the three algorithms are shown in Fig. 3(b), and these data in the high-T range are perfectly overlapped. However, as shown in the inset, the enlarged $U(T)$ data in the low-T range clearly demonstrate the effect of the energy cutoffs. Again, the rigorously predicted

$U(T)$ at the ground state should be $\varepsilon = -1.0$ [11]. The simulated result by the CWLS at $\varepsilon_c = -0.99$ deviates seriously from the rigorous prediction and the MMC result in the low-T limit. If $\varepsilon_c = -0.996$ is taken, one observes extremely long CPU time for the code running. However, for the MWLS, one has $\varepsilon_c = -0.995$, -0.998, and -0.999 at $N_w = 8$, 10, and 13, respectively, and therefore the data are sufficiently accurate to catch the lowest-T phase transitions if any ($T < 10^{-3}$).

B. Triangular J_2-J_2 spin model

Another model is the J_1-J_2 spin model on a triangular lattice. The Hamiltonian is $H = \Sigma_{<i,\,j>}[J_1\cos(\theta_{ij}) + J_2\cos(2\theta_{ij})]$, where $\langle i, j\rangle$ and θ_{ij} have the same definitions as those in the square XY model, $J_1 > 0$ is the antiferromagnetic interaction, and $J_2 > 0$ acts as nematic interaction which can lead to the nematic order [12,16]. To have a determined energy boundary, we set a constraint condition that $J_1 + J_2 = 1$, using parameter x ($0 \le x \le 1$) satisfying $J_1 = 1 - x$ and $J_2 = x$. Then this J_1-J_2 model has the ground energy $E_{\min} = -3/2N$ and $E_{\max} = 3N$. The normalized parameters are $\alpha = 3N/4$ and $\beta = 9N/4$. At $x > 0.7$, the model shows multiple phase transitions. Upon decreasing T, it goes from a paramagnetic phase (PM) to a phase with coexisting (antiferro) nematic (aN) order and chirality (C) order through the KT transition, and then from the coexisting aN and C orders to another phase with coexisting (antiferro) magnetic (aM) order and chirality order through the Ising transition at the critical point $T = T_c$ [12]. The latter one is usually very low for a small J_1/J_2 ratio, and continues to reduce as x tends close to 1.

In the present simulation, the low-T behaviors of this J_1-J_2 model with several small J_1/J_2 ratios are carefully studied using the three algorithms. The CWLS is performed with $\varepsilon_c = -0.9956$. One chooses $N_w = 13$ for the MWLS with $\varepsilon_c = -0.9999$. The MMC is performed from $T = 4.0$ to $T = 0.001$, using 10^6 MC steps to reach an equilibrium state and selecting 10^5 samples from the next 3×10^6 MC steps at each of the 100 T-data points. We carefully select three representative x values: $x = 0.95$, $x = 0.98$, and $x = 0.99$. The lattice has the Ising transition point T_c ($T_c \sim 0.0916$ for $x = 0.95$, $T_c \sim 0.0370$ for $x = 0.98$, and $T_c \sim 0.0184$ for $x = 0.99$), as derived from the fourth-order Binder cumulants scheme.

In Figs. 4(a)–4(c) are plotted the evaluated heat capacity $C(T)$ curves at the three x values, respectively. For each case, three different lattice sizes ($N = L^2$) are chosen for identifying the finite-size effect. For all the three x values, the $C(T)$ data from the MWLS show nearly perfect overlapping with those from the MMC, demonstrating the validity of the MWLS. However, for the CWLS, $\varepsilon_c = -0.9956$, remarkable difference from the MMC results is shown. The $C(T)$ exhibits rapid dropdown in the low-T side. The three $C(T)$ curves roughly cross at point T_d. At $x = 0.95$, $T_d \sim 0.0205 \ll T_c \sim 0.0916$, suggesting that the CWLS can reproduce the Ising transition well. At $x = 0.98$ where $T_c \sim 0.0370$, only slightly higher than $T_d \sim 0.0203$, the simulated $C(T)$ from the CWLS begins to show errors at $T \leqslant T_c$, implying that the Ising transition cannot be well described. At $x = 0.99$ where $T_c \sim 0.0184$, the obtained T_d from the CWLS is 0.0165, very close to T_c. In fact, the simulated $C(T)$ data are inconsistent with the correct results.

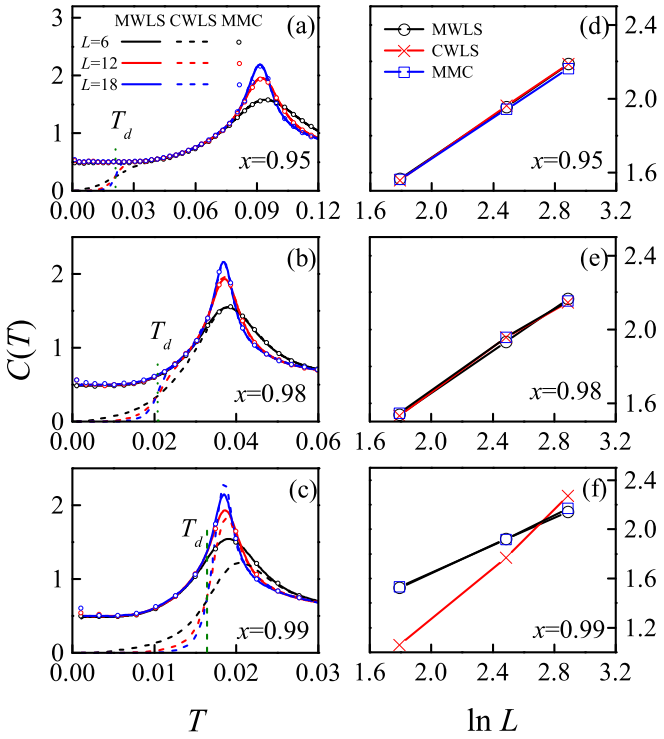

FIG. 4. (Color online) Calculated heat capacity $C(T)$ from the simulated DOS for the triangular J_1-J_2 model with $x = 0.95$ (a), 0.98 (b), and 0.99 (c), using the three different algorithms (MMC, CWLS, and MWLS with $N_w = 13$), respectively. The $C(T)$ as a function of $\ln L$ for $x = 0.95$ (d), 0.98 (e), and 0.99 (f), as evaluated from the data presented in (a), (b), and (c), respectively.

In addition, the dropdown behavior of the data from the CWLS in the low-T range also imposes significant impact on other properties of the Ising transition, such as the finite-size scaling. As demonstrated by Park *et al.* [12], the low-T phase transition from the nematic phase to the magnetic phase is Ising-like. For the 2D Ising phase transition, we have $C(L) = C_0 \ln L$ with scaling exponent $C_0 = 0.5$. In Figs. 4(e) and 4(f), the finite-size scaling is checked. For $x = 0.95$ and $x = 0.98$ where $T_c > T_d$, the scaling behaviors as evaluated from the CWLS and MWLS, respectively, are perfectly consistent with that evaluated from the MMC. However, for $x = 0.99$ where $T_c \sim T_d$, as shown in Fig. 3(f), the scaling exponent is $C_0 = 1.11$ from the CWLS, $C_0 = 0.56$ from the MWLS, and $C_0 = 0.57$ from the MMC, respectively. We can see that the C_0 from the CWLS already deviates remarkably from that from the MMC, while the C_0 from the MWLS is close to the MMC value, demonstrating the validity of the MWLS once more.

The validity of the MWLS can be further illustrated by the internal energy $U(T)$ data which perfectly overlap with those from the MMC, as shown in Fig. 5(b) for $x = 0.99$, while the $C(T)$ data are plotted in Fig. 5(a) for reference. The CWLS with $\varepsilon_c = -0.9956$ produces the $U(T)$ which begin to deviate from the MMC data at a temperature slightly higher than T_c. Unfortunately, below this point, $U(T) = \varepsilon_c$, which is obviously the artifact due to the insufficient energy cutoff of the CWLS. However, this problem can be substantially avoided in the MWLS which generates the $U(T)$ data perfectly overlapping with the MMC data even at $T < 0.001$. Surely, it

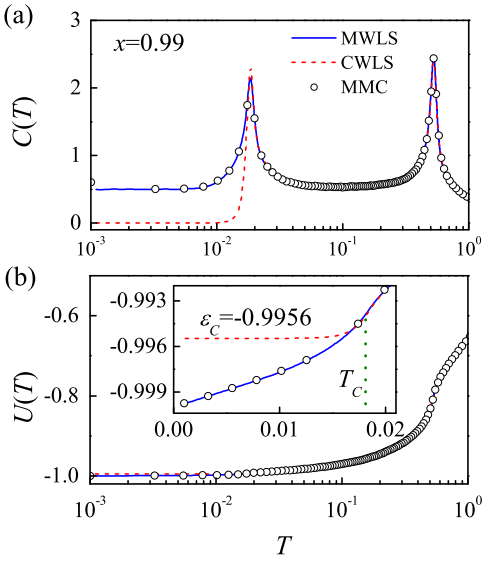

FIG. 5. (Color online) Calculated heat capacity $C(T)$ (a) and internal energy $U(T)$ (b) from the simulated DOS for the triangular J_1-J_2 model with $x = 0.99$ using the three different algorithms (MMC, CWLS, and MWLS with $N_w = 13$), respectively. The inset in (b) is the enlarged view of the low-T data. The ε_c is the energy cutoff value.

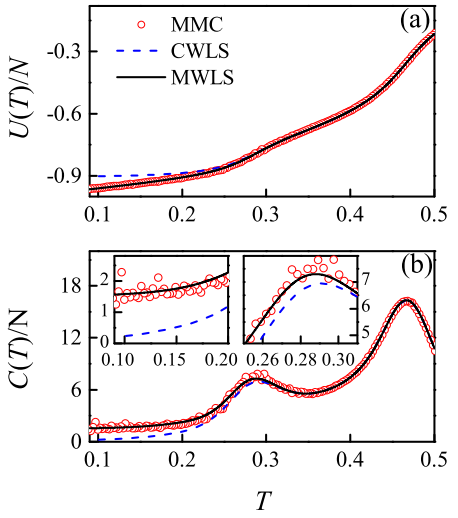

FIG. 6. (Color online) Calculated internal energy $U(T)$ (a) and heat capacity $C(T)$ (b) of the 13-atom Lennard-Jones cluster using the three different algorithms. The inset in (b) is the enlarged view of the low-T region (left) and the critical point region (right).

can be avoided too if the CWLS chooses an energy cutoff much closer to $\varepsilon_c = -1.00$; however, the CPU time for this computation becomes extremely long with very low computation efficiency.

C. Lennard-Jones cluster

The third model is a Lennard-Jones (LJ) cluster [17,18], which consists of the identical atoms gathered up by the LJ potential. Considering a cluster with N atoms, the LJ potential has the following form:

$$V_{\mathrm{LJ}} = \frac{1}{2}\sum_{i=1}^{N}\sum_{j=1,j\neq i}^{N} 4\varepsilon_0\left[\left(\frac{r_m}{r_{ij}}\right)^{12} - \left(\frac{r_m}{r_{ij}}\right)^{6}\right], \qquad (9)$$

where r_{ij} is the distance between atoms i and j, and ε_0 is the depth of the potential well and the $r = 2^{1/6}r_m$ is the equilibrium separation of the atom pairs. In our simulation, all the distances and energies are expressed in terms of the LJ parameters r_m and ε_0, while the LJ potential is cut off at distance $r_c = 6r_m$. We choose $N = 13$ cluster as an example. Thirteen is a small magic number for the Lennard-Jones clusters, and this cluster structure has been well demonstrated [17]. The ground state of the 13-atom cluster is stable and forms an icosahedron with 12 atoms located at the 12 vertices and one in the center. The ground energy is $E_{\min}/N = -3.40973\varepsilon_0$. Because the LJ potential has no top energy boundary, we must have a high-energy cutoff and the energy space considered here is restricted within $[E_{\min}, 0]$, and the normalized parameters are $\alpha = 0$ and $\beta = 3.40973\varepsilon_0 N$. It is noted that the high-temperature phase cannot be observed in the constant-temperature simulations due to the evaporation in infinite space. Here we restrict the atoms in a finite cubic box and employ the periodic boundary conditions, which correspond to the high-pressure environment. The box size is carefully chosen as $L = 10r_m > r_c$.

We employ the three algorithms to investigate this cluster model. It is noted that each atom is spatially defined by three degrees of freedom, while each spin in the XY spin model only has one degree of freedom. As a result, the MMC simulation is more easily affected by statistical fluctuations and thus needs more MC steps to reach the ground state. Here we run the codes for 10^8 Monte Carlo steps and make the sampling as big as 10^6 at each temperature point. As for the CWLS, we employ 4000 bins and energy cutoff $\varepsilon_c = -0.910$. A cutoff at $\varepsilon_c = -0.950$ has been tested and too much CPU time to be accessible in the present stage is needed. For the MWLS, we choose $N_w = 12$ with other control parameters identical to those used earlier.

The evaluated internal energy $U(T)$ and heat capacity $C(T)$ data are plotted in Figs. 6(a) and 6(b). The cluster has three different states at different T ranges: the liquid phase in the high-T range, solid phase in the low-T range, and the liquid-solid coexisting phase in the mid-T range, well consistent with earlier results [17]. These data provide additional proof that the MWLS is superior over the MMC and CWLS, given the assigned control parameters above. First, the insets in Fig. 6(b) evidence that the MWLS generates much better data quality than that from the MMC at temperatures as low as $T = 0.1$ and around the critical point, noting that the MMC data show remarkable fluctuations. Second, according to the classical equipartition theorem, the heat capacity would approach down to 1.5 as $T \to 0$, as reproduced by the MWLS data. However, the heat capacity data generated from the CWLS almost drop to zero at $T < 0.1$, seriously deviating from the rigorous prediction.

D. Comparison with analytic predictions

As mentioned earlier, the deficiency of the CWLS, if any, lies in the fact that the $g(\varepsilon)$ spectrum very close to the two end boundaries of the energy spectrum shows big errors, unless

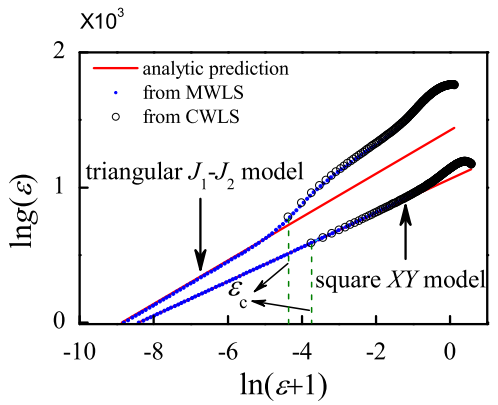

FIG. 7. (Color online) Simulated DOS ($\ln[g(\varepsilon)]$) as a function of $\ln(\varepsilon + 1)$ for the square XY model with $N = 16 \times 16$ and triangular J_1-J_2 model with $N = 18 \times 18$ at $x = 0.99$, using the CWLS and MWLS algorithms. The solid red lines are the predictions from the analytic models. The ε_c is the energy cutoff value.

a practically inaccessible energy cutoff $\varepsilon_c \to \pm 1.0$ is chosen. In this case, the CWLS is demonstrated to be very low in computational efficiency. This deficiency can be avoided in the MWLS, as shown above. In order to illustrate further the advantage of the MWLS, we discuss the $g(\varepsilon)$ spectrum very close to the boundaries. Fortunately, some rigorous results on the $g(\varepsilon)$ spectrum at $\varepsilon \sim -1.0$ for quite a few continuous models are available, which can be used to check the validity of the MWLS. We present in Fig. 7 the simulated $g(\varepsilon)$ from the CWLS and MWLS, as a function of $(\varepsilon + 1)$, for both the square XY spin model and the triangular J_1-J_2 spin model with $x = 0.99$. The analytical predictions which are rigorous for the two models in the $\varepsilon \sim -1.0$ limit are also plotted with solid lines [11].

For the square XY spin model, the $g(\varepsilon)$ spectrum in the $\varepsilon \sim -1.0$ limit can be expressed as $g(\varepsilon) = c(N)(\varepsilon + 1)^{(N-3)/2}$ with $c(N)$ a parameter independent of ε [11]. It is reasonable to observe the deviation of the simulated data from the predictions in the high energy far above the $\varepsilon \sim -1.0$ limit, since the analytical predictions fail there ($\varepsilon > e^{-2} - 1$). Due to the energy cutoff, no data in the $\varepsilon \sim -1.0$ limit are available from the CWLS, unless the chosen bin number is extremely big and the CPU time is extremely long. On the contrary, the MWLS can generate sufficiently accurate DOS data perfectly consistent with the analytic prediction even at $\varepsilon < e^{-8} - 1$, so close to $\varepsilon \sim -1.0$, as long as $N_w \geqslant 12$, which is an easily accessible task for the MWLS.

For the triangular J_1-J_2 spin model with $x = 0.99$, the MWLS simulated results agree very well with the prediction at $\varepsilon > e^{-5}$–1. The deviation in the high energy is again due to the fact that the model already fails in the high-energy case. While the CWLS can only generate the $g(\varepsilon)$ data at $\varepsilon > e^{-4}$–1 due to the energy cutoff, the MWLS can generate the data at $\varepsilon < e^{-8}$–1. The $g(\varepsilon)$ data at $\varepsilon < e^{-8}$–1 for the CWLS can be, in principle, obtained without objecting to the computational efficiency and CPU cost.

Actually, for quite a number of continuous systems, the $g(\varepsilon)$ spectrum near the ground state has a generalized form $\ln[g(\varepsilon)] \sim \ln(\varepsilon + 1)$. It is seen that term $\ln[g(\varepsilon)]$ tends to negative infinity as $\varepsilon \to -1.0$, which is the reason why one cannot choose $\varepsilon_c = -1.0$. To best describe the $g(\varepsilon)$ spectrum near the ground state, one should use a set of bins with logarithmically shrinking width to discretize the energy space. In the MWLS, the bin width does shrink logarithmically when the energy approaches the ground state; as a result this algorithm works well for the continuous models.

E. Computational efficiency

Finally, we discuss the computation efficiency issue. In a general sense, the CWLS can generate sufficiently accurate $g(\varepsilon)$ data, as long as no cost for the computation and efficiency is counted. The extremely low-T phase transition requires sufficiently accurate $g(\varepsilon)$ data near $\varepsilon = -1.0$. Unfortunately, as mentioned above, a cutoff very close to $\varepsilon \sim -1.0$ needs too much CPU time which may be impractical, in order to reach a "flat" histogram $H(\varepsilon)$. Here, we choose the triangular J_1-J_2 spin model with $x = 0.95$ as an example to discuss the computational efficiency issue for the three algorithms.

For measuring the computational efficiency, we set the time units for the simulations using the three algorithms, respectively. We start from a 6×6 lattice with $N = 6 \times 6$. For the CWLS, the energy cutoff is $\varepsilon_c = -0.9956$. It is observed that the CPU time needed is 4200 s which is the time unit for the CWLS. For the MWLS, we have $N_w = 13$ (the total bin number is $7800 > 4000$) and thus $\varepsilon_c = -0.9999$. The needed time for this simulation is 3800 s which is the time unit for the MWLS. For the MMC, the simulation is performed from $T = 4.0$ to $T = 0.001$, using 10^6 MC steps to reach an end state for each of 100 T-data points and then selecting 10^5 samples from the next 3×10^6 MC steps at this point. In this case, the needed CPU time is 4000 s which is the time unit for the MMC. It is noted that the three units are similar, allowing the following comparison.

Taking these time units as references to normalize the real CPU times needed for the simulations, we plot the CPU times using the three algorithms as a function of lattice size N, respectively, in Fig. 8 where each dot is an average over 20 independent runs and the statistical error bars are inserted too. It is seen that the time for the CWLS increases in an accelerated way and a very long time is needed for $N > 18 \times 18$. As for the MWLS, the time increases with N in an acceleration way too,

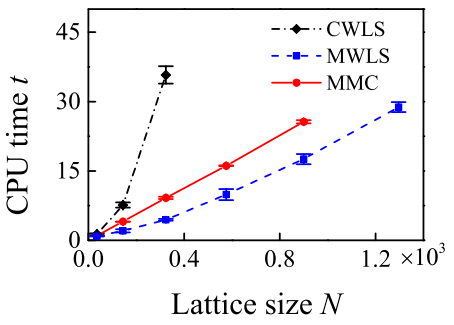

FIG. 8. (Color online) Evaluated CPU times needed for the triangular J_1-J_2 lattices with different sizes N ($x = 0.95$), using the three different algorithms (MMC, CWLS, and MWLS with $N_w = 13$), respectively. The CPU times are, respectively, normalized by the time units defined for a lattice of $N = 6 \times 6$.

but this acceleration is quite weak even for N up to 36×36. In a quantitative sense, the MWLS for $N = 36 \times 36$ needs 1.1×10^5 s, much shorter than 1.4×10^5 s for the CWLS with $N = 18 \times 18$. An extrapolation of the data for the CWLS predicts a CPU time of 20 days for $N = 36 \times 36$, while roughly 1 day is needed for the MWLS, noting that $\varepsilon_c = -0.9999$ for the MWLS and $\varepsilon_c = -0.9956$ for the CWLS. This demonstrates that the MWLS is indeed powerful with high efficiency of computation and suitable for large systems.

F. Discussion

So far, it has been revealed that the MWLS provides an accurate and efficient way to simulate the continuous models. In this work we only start from three simple continuous models to demonstrate the validity and high efficiency of the MWLS with respect to the CWLS. Additional and more complicated continuous models should be checked in the future.

There is no need to mention that this algorithm is not yet a perfect one, and several issues need to be addressed. First, the bottom boundary $E_{\min}$ should be determined in prior, which may not be always available. For a spin lattice, first, the spin configuration can be obtained via the Landau-Lifshitz-Gilbert equation using the micromagnetic simulation after an annealed Monte Carlo process [19], and $E_{\min}$ is the energy of such spin configuration. Second, in order to obtain an order of parameter m other than the energy parameter ε, the two-dimensional ε -m joint DOS $g(\varepsilon, m)$ should be simulated. For continuous spin models, this joint DOS simulation is an arduous task. Such difficulty may be avoided by calculating the $m(\varepsilon)$ spectrum using the WLS, but the challenge is still big [20]. For other continuous models, this algorithm may face more serious difficulties, which hints that additional strategy may be required for efficient and reliable simulations.

IV. CONCLUSIONS

In summary, we have developed a modified Wang-Landau sampling for continuous models. This algorithm is based on a partition of the whole energy space by a set of logarithmic energy windows. The success of this algorithm in acquiring a sufficiently accurate DOS spectrum for a square XY spin model and triangular J_1-J_2 spin model with extremely low-T phase transitions, as well as a Lennard-Jones cluster model of high degrees of freedom, has been described in detail. It is revealed that this modified Wang-Landau sampling makes a precise evaluation of the thermodynamic behaviors of continuous models accessible in efficient and accurate manners. The present work represents a substantial updating of the powerful Wang-Landau algorithm.

ACKNOWLEDGMENTS

This work was supported by the National 973 Projects of China (Grant No. 2011CB922101), the Natural Science Foundation of China (Grants No. 11234005, No. 11374147, and No. 51332006), and the Priority Academic Program Development of Jiangsu Higher Education Institutions, China.

[1] F. Wang and D. P. Landau, Phys. Rev. Lett. **86**, 2050 (2001).
[2] F. Wang and D. P. Landau, Phys. Rev. E **64**, 056101 (2001).
[3] D. P. Landau, S.-H. Tsai, and M. Exler, Am. J. Phys. **72**, 1294 (2004).
[4] N. Rathore and J. J. de Pablo, J. Chem. Phys. **116**, 7225 (2002).
[5] T. Wüst and D. P. Landau, Comput. Phys. Commun. **179**, 124 (2008).
[6] A. Troster and C. Dellago, Phys. Rev. E **71**, 066705 (2005).
[7] A. G. Cunha-Netto, A. A. Caparica, S.-H. Tsai, R. Dickman, and D. P. Landau, Phys. Rev. E **78**, 055701(R) (2008).
[8] T. Vogel, Y. W. Li, T. Wüst, and D. P. Landau, Phys. Rev. Lett. **110**, 210603 (2013).
[9] C. Zhou, T. C. Schulthess, S. Torbrügge, and D. P. Landau, Phys. Rev. Lett. **96**, 120201 (2006).
[10] C. Zhou and R. N. Bhatt, Phys. Rev. E **72**, 025701(R) (2005).
[11] J. Xu and H. R. Ma, Phys. Rev. E **75**, 041115 (2007).
[12] J.-H. Park, S. Onoda, N. Nagaosa, and J. H. Han, Phys. Rev. Lett. **101**, 167202 (2008).
[13] F. C. Poderoso, J. J. Arenzon, and Y. Levin, Phys. Rev. Lett. **106**, 067202 (2011).
[14] P. Poulain, F. Calvo, R. Antoine, M. Broyer, and P. Dugourd, Phys. Rev. E **73**, 056704 (2006).
[15] B. J. Schulz, K. Binder, M. Müller, and D. P. Landau, Phys. Rev. E **67**, 067102 (2003).
[16] D. H. Lee and G. Grinstein, Phys. Rev. Lett. **55**, 541 (1985).
[17] J. D. Honeycutt and H. C. Andersen, J. Phys. Chem. **91**, 4950 (1987).
[18] J. E. Jones and A. E. Ingham, Proc. R. Soc. London, Ser. A **107**, 636 (1925).
[19] *Introduction to the Theory of Ferromagnetism*, edited by A. Aharoni (Clarendon Press, Oxford, 1996).
[20] D. Jayasri, V. S. S. Sastry, and K. P. N. Murthy, Phys. Rev. E **72**, 036702 (2005).